PIER C

(Received 10 February 2026, Accepted 26 March 2026, Scheduled 21 April 2026)

A Low Mutual Coupling Dual-Band MIMO Antenna Based on Symmetrical Complementary Double-Split-Ring Resonators

Xuemei Zheng[1,*], Jiafu Xing[2], and Tongchao Zhang[2]

[1]*Key Laboratory of Modern Power System Simulation and Control and Renewable Energy Technology Ministry of Education, Northeast Electric Power University, Jilin, China*
[2]*Northeast Electric Power University, Jilin, China*

ABSTRACT: In this study, a novel symmetrical complementary double-split-ring resonator structure is proposed, operating in the frequency bands of 2.39–2.44 GHz (covering the core 2.4 GHz WLAN band) and 3.45–3.60 GHz (covering a key sub-band of n78 for 5G communications), to reduce the coupling of multiple-input multiple-output (MIMO) antennas within these two frequency bands. To align with the trend of antenna miniaturization, the inter-element spacing is only $0.08\lambda_0$. The measured results show that after loading the metamaterial, the antenna coupling in the operating bands is reduced by 0–10 dB and 8–23 dB, respectively, and the coupling in the two bands is below −17 dB and −27 dB, respectively. The peak gains achieved are 3.12 dBi and 4.51 dBi in the two bands. The ECC is less than 0.02, indicating excellent gain performance and effective decoupling capability of the MIMO antenna.

1. INTRODUCTION

In the wireless communication industry, antennas operating in a single frequency band can no longer meet the demands of various wireless application modules [1] in devices, due to rapid technological advancements. Currently, the 5th Generation Mobile Communication Technology (5G) [2] has been widely deployed in smart terminals. The combined operation of 5G and Wireless Local Area Network (WLAN) [3] within their respective independent frequency bands can further adapt to diversified application scenarios. As the number of mobile users increases dramatically, challenges arise regarding channel capacity and data transmission rates. Therefore, MIMO technology is employed to address this issue. Specifically, by utilizing the core spatial multiplexing technique [4] of MIMO technology, multiple independent data streams [5] are transmitted simultaneously within the same frequency band. This increases antenna capacity, consequently enhancing the data transmission rate.

In addition, current intelligent terminal devices are evolving toward miniaturization [6]. As a result, the space reserved for antennas is gradually constrained during device integration, and reducing the spacing between MIMO antenna elements serves as an effective solution to shrink the antenna footprint. Coupling effects inherently exist among MIMO antennas, and excessively close proximity between antenna elements will induce severe electromagnetic mutual coupling [7], which severely deteriorates the radiation performance of the antennas. Simultaneously satisfying the requirements of smaller inter-element spacing and lower mutual coupling between antennas imposes more stringent demands on antenna design.

To date, the mainstream techniques for mitigating inter-antenna coupling include Defected Ground Structure (DGS) [8], Electromagnetic Band Gap (EBG) [9], neutralization lines [10], reconfigurable antenna structures [11], and metamaterials [12]. Metamaterials are novel, artificially synthesized periodic structures. The novel complementary split-ring resonator structure proposed in this paper exploits its distinctive electromagnetic characteristics at 2.4 GHz and 3.5 GHz, and significantly enhances the isolation between dual-band MIMO antennas without increasing the overall dimensions of the antenna structure.

This paper presents the design, simulation, and testing of a low coupling, dual-band, two-port MIMO antenna based on metamaterials, targeting the 2.39–2.44 GHz (covering the core 2.4 GHz WLAN band) and 3.45–3.60 GHz (covering a key sub-band of n78 for 5G communications) frequency bands. A mutually symmetric, double-split semicircular complementary metamaterial structure is placed between two original "concave"-shaped patch antenna elements to reduce inter-element coupling at the two specific frequency bands. While ensuring that the operational bands remain unchanged before and after introducing the metamaterial, the port isolation between antenna elements exceeds 22 dB across both working bands. The antenna structure and overall dimensions were analyzed and optimized using electromagnetic simulation software (HFSS). Subsequently, a physical prototype was fabricated and measured to verify the consistency with the simulation results.

2. DUAL-BAND MIMO ANTENNA DESIGN

The MIMO antenna designed in this paper targets center operating frequencies of 2.4 GHz and 3.5 GHz. By examining the

* Corresponding author: Xuemei Zheng (zhengxuemei@neepu.edu.cn).

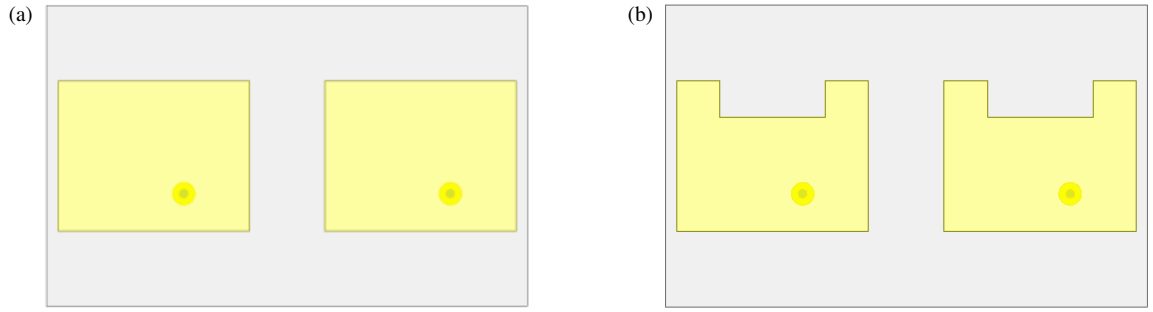

FIGURE 1. Design process of the dual-band MIMO antenna: (a) Rectangular structure; (b) Modified structure.

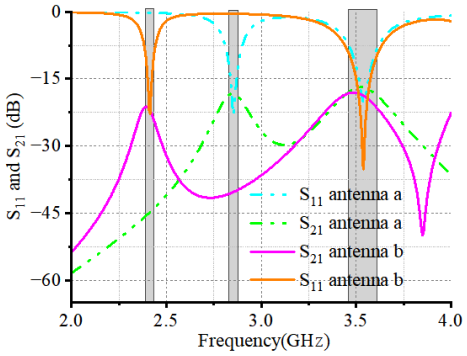

FIGURE 2. Comparison of MIMO antenna performance optimization.

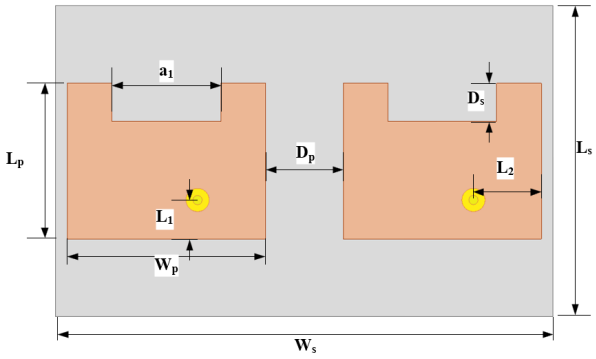

FIGURE 3. Configuration of the dual-band MIMO antenna.

TABLE 1. Geometric parameters of the antenna (Unit: mm).

Parameter	Reference Value	Parameter	Reference Value
a	9.7 mm	W_p	25.5 mm
R_1	4 mm	L_1	5 mm
g_1	0.6 mm	L_2	8.8 mm
g_2	0.2 mm	a_1	14 mm
w_1	0.2 mm	D_s	4.8 mm
w_2	0.7 mm	D_p	10 mm
w_3	0.9 mm	L_s	40 mm
W_s	64 mm	L_p	20.4 mm

S-parameters shown in Figure 2, it can be observed that although the high-frequency band meets the design requirements, the low-frequency band consistently fails to reach 2.4 GHz. To precisely control the antenna's resonance, particularly to lower the resonant frequency in the low band, this study introduces a rectangular slot structure. The evolution process is shown in Figure 1. The introduction of this structure essentially creates a controlled geometric perturbation on the radiator. This alters the distribution path and density of the surface current on the antenna, effectively adjusting its equivalent electrical length and enabling the fine-tuning of the resonant frequency.

All the above radiating patches are printed on the front side of the dielectric substrate. The backside is a ground plane fully covering the substrate (material: FR-4, relative permittivity: 4.4, loss tangent: 0.005), facilitating more convenient fabrication of the physical prototype. The dimensions of the dielectric substrate are $64 \times 40 \times 1.6\,\text{mm}^3$. Figure 3 and Table 1 present the detailed dimensional information of the designed antenna.

3. METAMATERIAL ANALYSIS

To extract effective electromagnetic parameters, the most commonly used waveguide simulation method was employed for the metamaterial unit. Figure 4 shows the designed metamaterial unit structure, which is placed on the top surface of a substrate with a thickness of 1.6 mm, and the entire structure is placed inside an air box.

To simulate the magnetic resonance generated when a magnetic field passes through the metamaterial structure, it was nec-

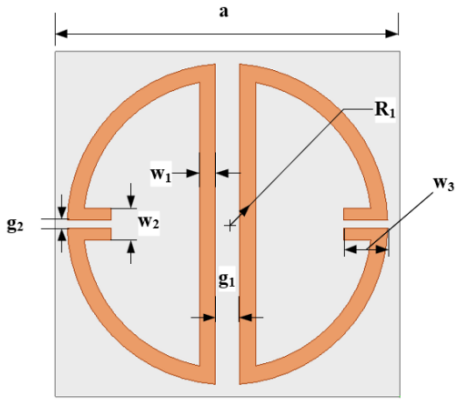

FIGURE 4. Structure of the symmetric complementary double-split-ring resonator unit.

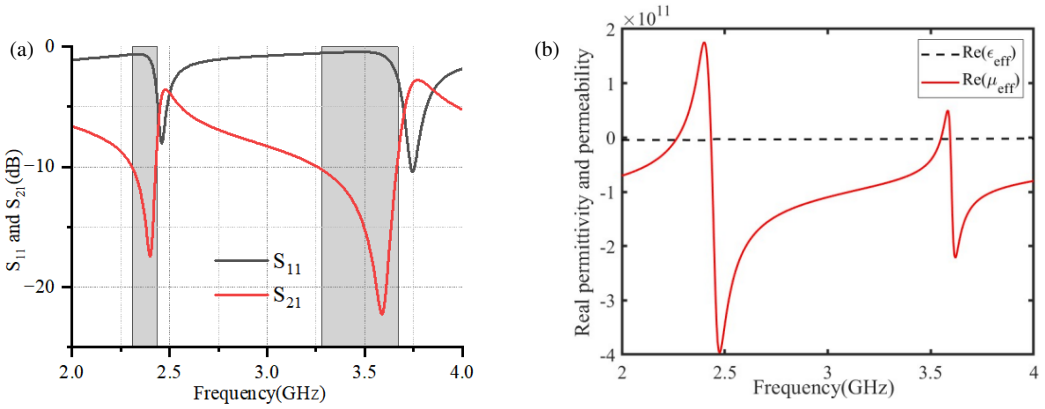

FIGURE 5. (a) S_{11} and S_{21} curves obtained from waveguide simulation; (b) Extracted equivalent electromagnetic parameter.

essary to orient the magnetic field perpendicular to the surface of the metamaterial unit. The simulation model was configured accordingly: the boundaries in the top and bottom directions were set as perfect magnetic conductors (PMCs), the boundaries in the front and back directions were set as perfect electric conductors (PECs), and the boundaries on the left and right sides were set as wave port excitations.

Using HFSS electromagnetic simulation, the reflection coefficient (S_{11}) and transmission coefficient (S_{21}) of the metamaterial unit can be obtained, as shown in Figure 5(a). It can be clearly observed that the metamaterial exhibits transmission stopbands around both 2.4 GHz and 3.5 GHz, indicating that the metamaterial unit structure presents high impedance to the coupled surface currents. At these frequencies, the frequency of the incident electromagnetic wave matches the resonant frequency, enabling the metamaterial to absorb or scatter the coupled electromagnetic wave energy between the antenna elements. This is visually verified by the surface current distribution shown in Figure 10. As a result, the coupling paths can be interrupted to achieve decoupling in MIMO antennas without significantly altering the reflection coefficient.

To verify the electromagnetic characteristics of the proposed metamaterial structure — specifically, whether the permeability and permittivity are negative — the S-parameters of the metamaterial unit were first extracted from HFSS simulation results. These data were then imported into a MATLAB program and calculated using a parameter extraction algorithm to more clearly present the equivalent electromagnetic parameter curves, as shown in Figure 5(b).

The final results indicate that the proposed split-ring resonator exhibits negative permeability at 2.4 GHz and 3.5 GHz, and negative permittivity throughout the 2–4 GHz range. Consequently, it can be characterized as a double-negative metamaterial unit at both 2.4 GHz and 3.5 GHz.

4. DUAL-BAND LOW-COUPLING MIMO ANTENNA

The finalized dual-band low-coupling MIMO antenna is shown in Figure 6. Based on the aforementioned MIMO antenna structure, the introduced metamaterial units are positioned in a 1×3 array and arranged as complementary structures, with their specific positions shown in Figure 6. They are placed in a waveguide configuration at the central position on the same surface as the MIMO antenna elements. In the figure, $L = 8.8\,\text{mm}$, $W = 27.2\,\text{mm}$, and the spacing between two adjacent metamaterial units is $m_1 = 0.5\,\text{mm}$. To ensure the credibility of the comparison between results before and after the introduction of the metamaterial, it is essential to guarantee that the dimensions and structure of the MIMO antenna remain unchanged.

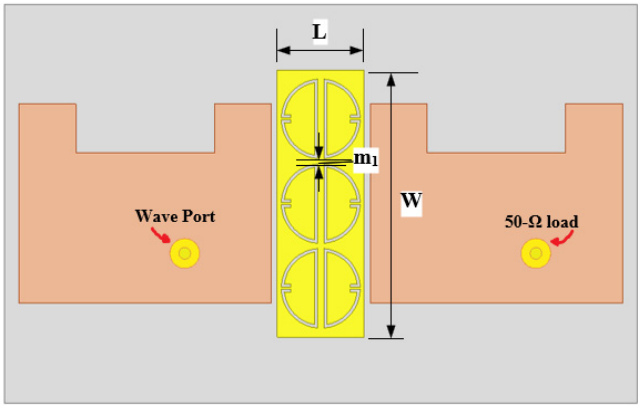

FIGURE 6. Planar configuration of the MIMO antenna.

4.1. Analysis of S-Parameters

Figures 7(a) and (b) show the comparison of S_{11} and S_{21} parameters before and after integrating the complementary split-ring resonator array structure. The reflection coefficient shows minimal variation; the bandwidth of the MIMO antenna remains largely unaffected, with only a slight shift of the operating frequency in the high-frequency band, which is essentially negligible. Observing the transmission coefficient reveals a significant impact at the two frequencies of 2.4 GHz and 3.5 GHz after incorporating the metamaterial. The mutual coupling of the MIMO antenna is notably improved: coupling is reduced by $-14\,\text{dB}$ at 2.4 GHz and by $-23\,\text{dB}$ at 3.5 GHz. Overall, the mutual coupling across the operating bands remains below $-22\,\text{dB}$. This result aligns well with the conclusion drawn from the analysis of the stopband characteristics, highlighting the unique advantage of metamaterials in multi-band decoupling.

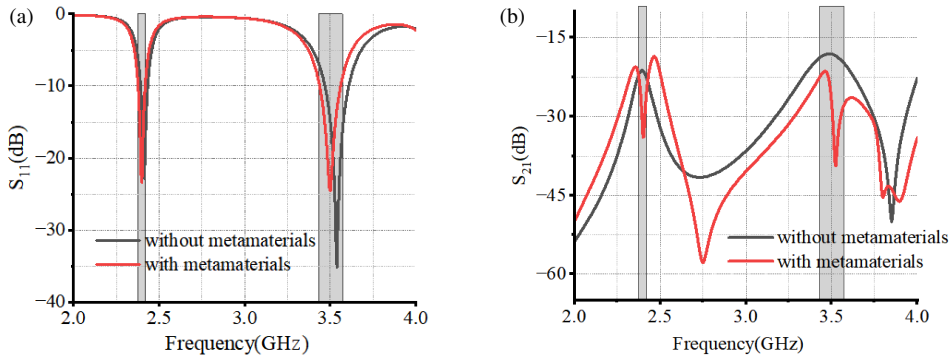

FIGURE 7. Comparison of S-parameters with and without metamaterial: (a) S_{11}, (b) S_{21}.

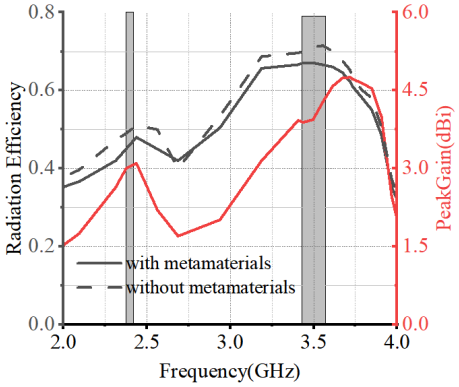

FIGURE 8. Peak gain and radiation efficiency curves of the dual-band MIMO antenna.

4.2. Antenna Radiation Performance

As shown in Figure 8, for the dual-band MIMO antenna loaded with the metamaterial, the gain ranges from 2.99 to 3.12 dBi in the low-frequency band (2.39–2.44 GHz), with a radiation efficiency ranging from 45% to 48%. In the high-frequency band (3.45–3.60 GHz), the gain ranges from 3.93 to 4.51 dBi, and the radiation efficiency ranges from 66% to 67%. This agrees with the values highlighted in the abstract.

The left side of Figures 9(a) and 9(b) represents the H-plane, while the right side represents the E-plane of the radiation patterns. Figure 9 compares the simulated radiation patterns (E-plane and H-plane) of the MIMO antenna at 2.4 GHz and 3.5 GHz, with and without the metamaterial structure. It can be observed that the introduction of the metamaterial structure does not significantly alter the radiation characteristics of the antenna. The patterns remain nearly identical, exhibiting only minor variations. To provide a more comprehensive perspective and further demonstrate the stability of the radiation patterns, Figure 10 presents the 3D radiation patterns at both frequencies with and without the metamaterial. The 3D views confirm that the overall radiation shape and directionality are preserved.

This confirms that the decoupling structure effectively reduces mutual coupling without distorting the far-field radiation pattern of the antenna, all of which demonstrates that the designed MIMO antenna possesses excellent radiation performance.

4.3. Antenna Surface Current Distribution

To more intuitively demonstrate the decoupling effect of the metamaterial on the MIMO antenna, the surface current distributions of the MIMO antenna at 2.4 GHz and 3.5 GHz are analyzed below. To ensure rigorous comparison, an identical scale is used for the current magnitude legend.

The current distribution comparison is shown in Figure 11. In the simulation setup, Port 1 on the left side of the MIMO antenna is excited, while Port 2 on the right side is terminated with a 50-ohm impedance load. This configuration is used to study the interference from Antenna Element 1 to Element 2 under the influence of the decoupling structure. In the figures, darker color indicates stronger coupling current between the antenna elements, and lighter color indicates weaker coupling. By observing Figure 11, it can be seen that the metamaterial array provides varying degrees of decoupling at the two frequencies by absorbing the coupled electromagnetic energy.

4.4. Diversity Characteristics of the Antenna

To further evaluate the performance of the MIMO antenna, two metrics, the Envelope Correlation Coefficient (ECC) and Diversity Gain (DG), are introduced to analyze its diversity performance. Good diversity performance effectively suppresses signal fading, thereby enhancing transmission efficiency and reliability. ECC is a key metric in this evaluation. In simple terms, a lower ECC value indicates less interference between antenna elements when they operate independently. A value below 0.05 is generally considered a common benchmark. The ECC value is calculated using formula (1) [20]:

$$\mathrm{ECC} = \frac{\left|S_{11}^{*}S_{12}^{'} + S_{21}^{*}S_{22}^{'}\right|^{2}}{\left(1-\left(|S_{11}|^{2}+|S_{21}|^{2}\right)\right)\left(1-\left(|S_{22}|^{2}+|S_{12}|^{2}\right)\right)} \tag{1}$$

Here, S_{11}^{*} and S_{21}^{*} refer to the imaginary parts of S_{11}^{*} and S_{21}^{*}, respectively, while $S_{12}^{'}$ and $S_{22}^{'}$ refer to the real parts of S_{12} and S_{22}.

Furthermore, as another key reference indicator for evaluating the diversity performance of MIMO antennas, Diversity Gain (DG) differs from ECC in that a larger DG value indicates better antenna diversity performance. Formula (2) [21] for cal-

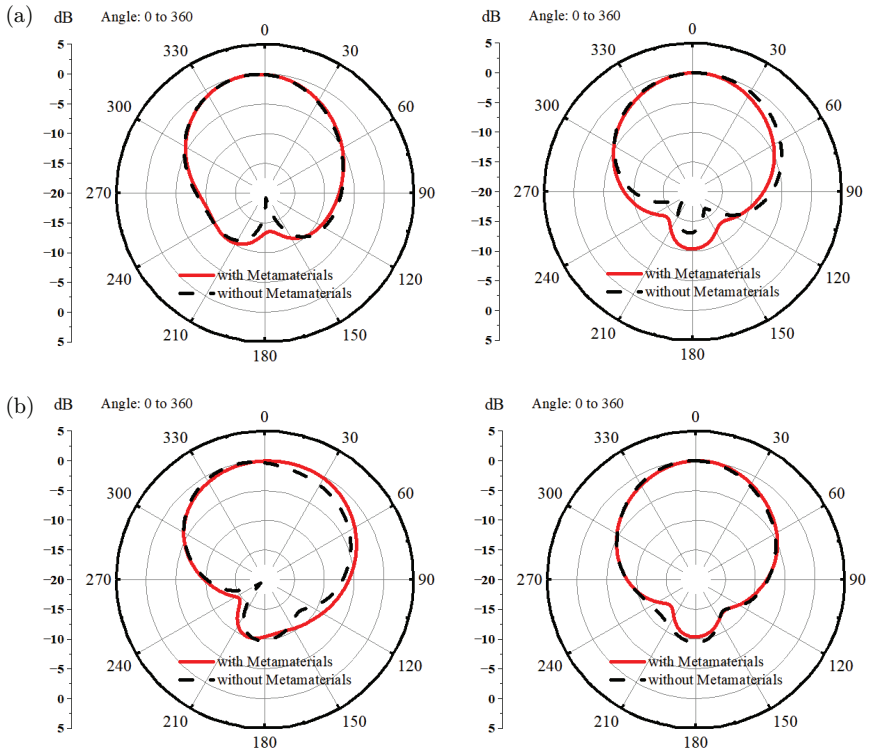

FIGURE 9. H-plane (left) and E-plane (right) radiation patterns of the dual-band antenna array with and without the metamaterial: (a) at 2.4 GHz, (b) at 3.5 GHz.

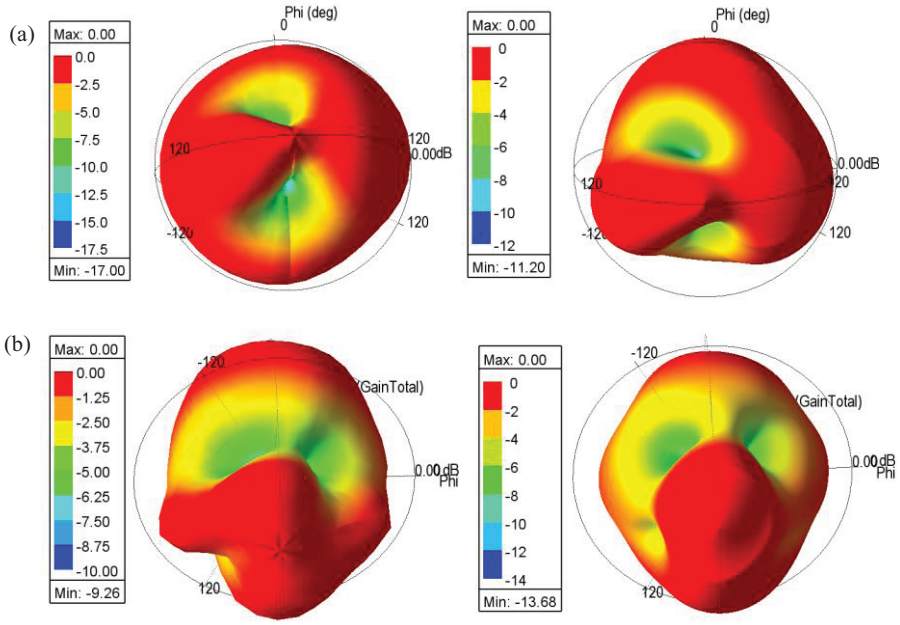

FIGURE 10. 3D radiation patterns of the dual-band antenna without (left) and with (right) the metamaterial (unit: dB): (a) at 2.4 GHz, (b) at 3.5 GHz.

culating the ECC value is shown below:

$$\mathrm{DG} = 10\sqrt{1 - \mathrm{ECC}} \tag{2}$$

Based on the simulation results of the ECC and DG curves shown in Figure 12, the designed dual-band MIMO antenna meets the design requirements for both metrics. The antenna achieves a DG of 9.9 dBi in both frequency bands, while its ECC remains below 0.02. This further confirms that the designed MIMO antenna maintains excellent isolation across both operational bands.

4.5. Comparative Analysis of the Antenna

As shown in Table 2, compared with [13–19], all the MIMO antennas listed are dual-band low-coupling designs. A comparison with [13] and [19] shows that although the proposed

TABLE 2. Performance comparison of the proposed MIMO antenna and antenna structures in the literature.

Reference	Size (mm)	Center Frequency (GHz)	Bandwidth (GHz)	Max. Isolation $\lvert S_{21}\rvert$ (dB)	Gain (dBi)	ECC
[13]	$60 \times 60 \times 1.6$	2.74	2.42–3.07	34	2.8	< 0.01
		5.25	4.14–6.07	26	4.91	< 0.005
[14]	$40 \times 47.5 \times 1.5$	2.45	2.2–2.83	20.7	1.99	< 0.017
		5.55	5.03–5.95	42.6	3.71	< 0.004
[15]	$40 \times 40 \times 1.6$	3.5	3.46–3.56	20	1.63–1.74	< 0.02
		5.3	5.22–5.41	22	4.07–5.05	< 0.01
[16]	$52 \times 40 \times 1.6$	3.4	3.37–3.40	20	NG	NG
		4.95	5.2–5.35			
[17]	$54 \times 42 \times 1.6$	2.4	2.38–2.44	20	NG	< 0.1
		5.3	5.2–5.36			
[18]	$55 \times 42 \times 1.6$	5.4	5.00–5.8	20	NG	< 0.05
		6.8	6.60–7.00			
[19]	$120 \times 68 \times 8$	2.4	2.25–2.63	15.3	5.1	< 0.05
		5	5.14–6.06		7.8	< 0.1
This paper	$64 \times 40 \times 1.6$	2.4	2.39–2.44	3	2.99–3.12	< 0.02
		3.5	3.45–3.60	38	3.93–4.51	< 0.01

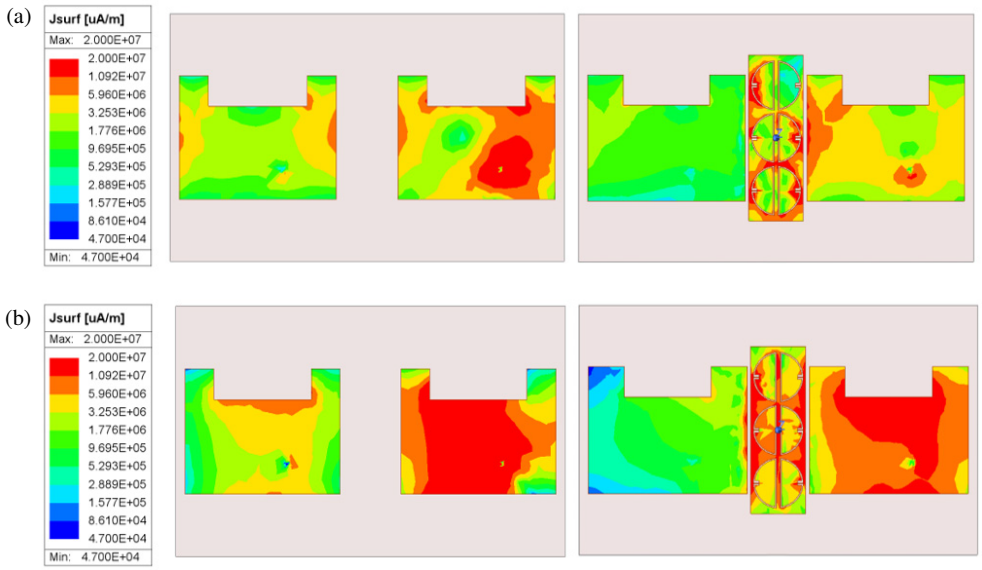

FIGURE 11. Comparison of current distribution: (a) @2.4 GHz, (b) @3.5 GHz.

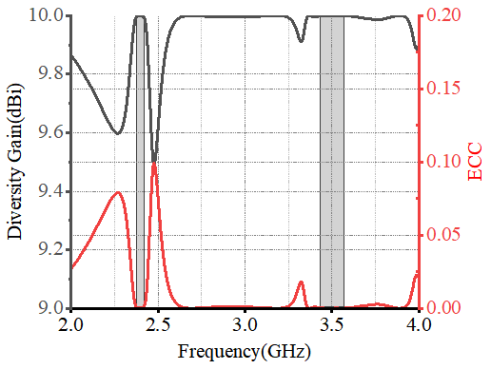

FIGURE 12. Peak gain and radiation efficiency curves of the antenna loaded with metamaterial.

antenna has a slightly narrower bandwidth, its compact size aligns well with the trend of antenna miniaturization. Ref. [14] demonstrates clear advantages in terms of both isolation and ECC performance; however, its relatively low gain makes it less suitable for modern mobile communication requirements. Furthermore, compared to the proposed antenna, Refs. [15–18] achieve a reduction in overall antenna size, but their maximum isolation is only around 20 dB, indicating a less significant effect in reducing inter-element coupling. It is worth noting that Ref. [16] has an even narrower bandwidth than the proposed design, while the ECC value in [17] is too high to meet the existing standard of ECC < 0.05. Therefore, the proposed MIMO antenna structure offers a comprehensive advantage in terms of

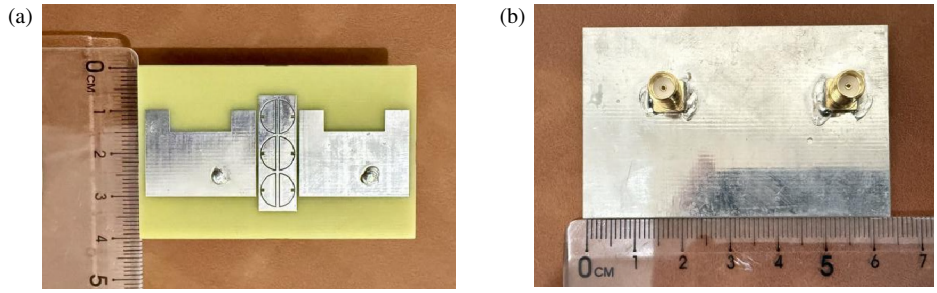

FIGURE 13. Fabricated prototype photograph of the MIMO antenna: (a) Front view, (b) back view.

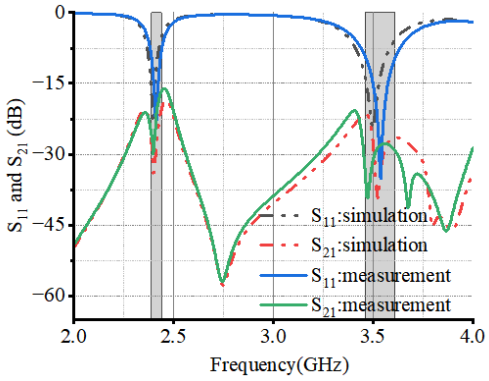

FIGURE 14. Comparison of measured and simulated S-parameters for the MIMO antenna.

size, bandwidth, isolation, gain, and ECC performance, making it suitable for a wider range of communication scenarios.

5. MEASUREMENT AND RESULTS OF THE MIMO ANTENNA

To verify the reliability of the simulation results, a physical model of the MIMO antenna was fabricated based on the design from the electromagnetic simulation software HFSS, as shown in Figure 13. It can be clearly seen that the decoupling structure consists of three complementary split-ring resonators etched on the ground plane between the two antenna elements, with the entire antenna integrated on a 1.6 mm FR-4 substrate. The S-parameters of the fabricated MIMO antenna were then measured using an Agilent Vector Network Analyzer (VNA). The measurement results are shown in Figure 14. While slight discrepancies exist between the measured S_{21} and S_{11} results and their simulated counterparts, three primary potential reasons for these differences are analyzed below: Firstly, the connection between the transmission line ends on the back of the substrate and the SMA connectors may not have been perfectly secure. Secondly, fabrication tolerances in the dielectric substrate could have affected the radiation performance. Finally, measurement noise and external electromagnetic interference in the testing environment may have contributed to the variations.

Overall, the errors introduced by the factors above are within an acceptable range and did not substantially affect the physical measurement results. The measured results are in good agreement with the simulated ones. The measurements show that the coupling in the two bands is below -17 dB and -27 dB within the 2.4 GHz and 3.5 GHz operating bands, respectively, demonstrating excellent isolation across the two frequency bands.

6. CONCLUSION

In this design, a compact, low-coupling dual-band MIMO antenna system based on a symmetrical complementary double-split-ring resonator is proposed. By integrating a 1×3 metamaterial array between the radiating elements, an inter-element spacing of only $0.08\lambda_0$ is achieved without increasing the overall size, offering a notable advantage in miniaturization. The antenna operates in the 2.39–2.44 GHz (covering the core 2.4 GHz WLAN band) and 3.45–3.60 GHz (covering a key sub-band of n78 for 5G communications) bands, with measured gains of 2.99–3.12 dBi and 3.93–4.51 dBi, respectively, and a diversity gain greater than 9.9 dBi. The envelope correlation coefficient remains below 0.02 across both bands. The measured results demonstrate that incorporating the novel metamaterial structure reduces antenna coupling by 0–10 dB and 8–23 dB in the two operating bands, respectively, resulting in coupling levels below -17 dB and -27 dB, confirming the effective decoupling capability of the proposed structure.

In summary, the proposed MIMO antenna not only maintains good gain and radiation performance but also achieves independent tuning of the decoupling responses at 2.4 GHz and 3.5 GHz through the use of novel complementary split-ring resonators. This fills the research gap in the application of metamaterials for this specific dual-band combination and further expands the application research of metamaterials for decoupling in closely spaced multi-band MIMO antennas.

ACKNOWLEDGEMENT

This paper was funded by the National Natural Science Foundation of China (61803356). This paper was supported by the Jilin Provincial Department of Education Science Research Project, with the project number JJKH20261429KJ.

REFERENCES

[1] Jemaludin, N. H., R. H. Elabd, A. Gupta, T. Addepalli, H. Singh, T. Saeidi, Z. Zakaria, and A. J. A. Al-Gburi, "Compact MIMO antenna with metamaterial-based S-line decoupling stub for high

isolation and multiband applications," *Results in Optics*, Vol. 21, 100926, 2025.

[2] Hussain, R. and M. S. Sharawi, "5G MIMO antenna designs for base station and user equipment: Some recent developments and trends," *IEEE Antennas and Propagation Magazine*, Vol. 64, No. 3, 95–107, 2022.

[3] Dev, P., S. K. Gupta, A. Bage, and L. Murmu, "High isolated MIMO antenna for WLAN applications," *Journal of Circuits, Systems and Computers*, Vol. 31, No. 6, 2250109, 2022.

[4] Zheng, X., Z. Zhao, Y. Zhang, T. Zhang, A. Gui, and H. Wu, "A low-coupling broadband MIMO array antenna design for Ku-band based on metamaterials," *Journal of Electromagnetic Engineering and Science*, Vol. 24, No. 6, 666–673, 2024.

[5] Zheng, X., Z. Zhao, Y. Pan, and T. Zhang, "Design of a miniaturized symmetrical E-shaped MIMO antenna with low coupling," *Applied Computational Electromagnetics Society Journal (ACES)*, Vol. 39, No. 12, 2024.

[6] Khadar, S. A. and S. Sahu, "Compact metamaterial loaded wideband monopole antenna for wireless applications," *Progress In Electromagnetics Research C*, Vol. 128, 247–261, 2023.

[7] Zheng, X., L. Yue, and Y. Zhang, "A compact four-port axially symmetric UWB-MIMO antenna array: Metamaterial-integrated coplanar waveguide for broadband operation with high isolation," *Progress In Electromagnetics Research C*, Vol. 162, 58–69, 2025.

[8] Qian, B., X. Huang, X. Chen, M. Abdullah, L. Zhao, and A. A. Kishk, "Surrogate-assisted defected ground structure design for reducing mutual coupling in 2×2 microstrip antenna array," *IEEE Antennas and Wireless Propagation Letters*, Vol. 21, No. 2, 351–355, 2022.

[9] Wu, W., B. Yuan, and A. Wu, "A quad-element UWB-MIMO antenna with band-notch and reduced mutual coupling based on EBG structures," *International Journal of Antennas and Propagation*, Vol. 2018, No. 1, 8490740, 2018.

[10] Zhou, J., M. Yang, and Z. Wang, "MIMO antenna system with wideband, high isolation and directional radiation characteristics by using multi-functional neutralization line," *Physica Scripta*, Vol. 100, No. 10, 105501, 2025.

[11] Beneck, R. J., A. Das, G. Mackertich-Sengerdy, R. J. Chaky, Y. Wu, S. Soltani, and D. Werner, "Reconfigurable antennas: A review of recent progress and future prospects for next generation," *Progress In Electromagnetics Research*, Vol. 171, 89–121, 2021.

[12] Tadesse, A. D., O. P. Acharya, and S. Sahu, "Application of metamaterials for performance enhancement of planar antennas: A review," *International Journal of RF and Microwave Computer-Aided Engineering*, Vol. 30, No. 5, e22154, 2020.

[13] Abhilash, A., P. Thomas, K. K. Indhu, K. Neema, R. A. Kumar, and C. Aanandan, "Four-element compact and dual-band MIMO antenna with self-decoupled mechanism for 5G applications," *Progress In Electromagnetics Research C*, Vol. 123, 91–99, 2022.

[14] Yahya, L. S., L. S. Yahya, and K. H. Sayidmarie, "A crescent-shaped monopole MIMO antennas with improved isolation for dual-band WLAN applications," *Progress In Electromagnetics Research C*, Vol. 117, 115–127, 2021.

[15] Zheng, X., Z. Zhao, and Y. Pan, "Compact dual-band MIMO antenna with complementary isotropic open resonant ring for mutual coupling reduction," *Journal of Electromagnetic Engineering and Science*, Vol. 26, No. 1, 10–17, 2026.

[16] Guo, C., H. Zhai, and S. Liu, "A new dual-band microstrip antenna array with high isolation by waveguided metamaterial structure," *Microwave and Optical Technology Letters*, Vol. 61, No. 5, 1365–1370, 2019.

[17] Luo, S., Y. Li, and W. Shi, "A dual-frequency antenna array with mutual coupling reduction via metamaterial structures," in *2018 IEEE International Symposium on Antennas and Propagation & USNC/URSI National Radio Science Meeting*, 1385–1386, Boston, MA, USA, 2018.

[18] Talha, M. Y., K. J. Babu, and R. W. Aldhaheri, "Design of a compact MIMO antenna system with reduced mutual coupling," *International Journal of Microwave and Wireless Technologies*, Vol. 8, No. 1, 117–124, 2016.

[19] Zhang, W., Y. Li, K. Wei, and Z. Zhang, "A dual-band MIMO antenna system for 2.4/5 GHz WLAN applications," *IEEE Transactions on Antennas and Propagation*, Vol. 71, No. 7, 5749–5758, 2023.

[20] Manikonda, R., G. Tamminaina, and S. Gulla, "Design and analysis of high isolation four port MIMO antenna for N77 band 5G communication," *Progress In Electromagnetics Research C*, Vol. 163, 35–42, 2025.

[21] Elalaouy, O., B. Aghoutane, M. El Ghzaoui, S. Das, J. Foshi, and H. El Faylali, "High isolation and gain metamaterial based MIMO antenna for 5G millimiter wave applications," in *2024 International Conference on Circuit, Systems and Communication (ICCSC)*, 1–6, Fes, Morocco, 2024.